Desalination and Water Treatment
www.deswater.com
doi: 10.5004/dwt.2022.28385

256 (2022) 289–299
April

High efficiency adsorption of Disperse Red 167 dye by Mg-Fe bimetallic oxide@biochar composites

Huifang Wang, Boya Wang, Wenwen Zhou, Baowei Hu, Muqing Qiu*

College of Life Science, Shaoxing University, Shaoxing 312000, China, email: qiumuqing@usx.edu.cn (M. Qiu)

Received 6 October 2021; Accepted 24 February 2022

ABSTRACT

The dye wastewater was considered as a kind of harmful environmental pollutant. It would destroy the ecological environment, and formed carcinogens affecting human health. Therefore, it was very urgent to treat dye wastewater efficiently. In this work, the novel Mg-Fe bimetallic oxide@biochar composites (Mg-Fe@BC) were prepared from peanut shell by the chemical method of microwave-assisted hydrothermal. The adsorption of Disperse Red 167 dye (DR 167 dye) by Mg-Fe@BC was carried out in a serial of adsorption experiments. The characterization of Mg-Fe@BC was characterized by Fourier-transform infrared spectroscopy, X-ray diffraction, transmission electron microscopy and scanning electron microscopy-energy-dispersive X-ray spectroscopy. The results showed that biochar was successfully loaded by the Mg-Fe bimetallic oxide nanoparticles. The adsorption capacity of DR 167 dye by Mg-Fe@BC was higher than that of the unmodified biochar. The removal rate of DR 167 dye by Mg-Fe@BC could reach 92.7%. The functional groups (such as O–H, C=C or C–C, COO– and C–O–C) could be observed on the surface of Mg-Fe@BC. The adsorption kinetics of DR 167 dye by Mg-Fe@BC was fitted with pseudo-second-order kinetic and Langmuir models. The proposed mechanisms of DR 167 dye removal by Mg-Fe@BC involved surface complexation, π–π interaction, hydrogen bond and electrostatic attraction.

Keywords: Adsorption; Disperse Red 167; Mg-Fe bimetallic oxide@biochar composites; Mechanism

1. Introduction

Water resources are indispensable resources in people's daily life [1,2]. With the rapid development of industrialization, such as paper manufacturing [3], textile [4], food [5] and energy mining [6], pollutants have brought great challenges to the water environment and aggravated the shortage of water resources. In recent years, about 280,000 tons of industrial wastewater containing dyes wastewater were discharged into the environment every year [7]. Azo dye pollution was particularly prominent in water pollution because of its complex composition, high chroma and poor biodegradability. Therefore, it was also one of the most difficult treatments of contaminants [8,9]. In general, different chromophores in the molecular structure of dyes could make the dyes in color, such as carbonyl (–C=O–), nitro (–N=O–) groups, etc. [10]. Azo dyes were widely used in many industries because of their unique azo chromophore (–N=N–) [11]. Disperse Red 167 (DR 167) dye was used widely because of its bright color and strong color fastness. However, DR 167 dye could cause the changes of structure and function in human cells [12]. Therefore, the effective removal of DR 167 dye was very important.

Nowadays, a variety of treatment technologies have been used to treat azo dye wastewater, such as ion exchange [13], bioremediation [14], solvent extraction [15]

* Corresponding author.

and adsorption [16,17]. Among those technologies, chemical treatment methods were limited by complex reaction conditions, high cost and secondary pollution. Therefore, removal of wastewater pollution economically and effectively is a major issue of environmental protection [18,19]. Recent studies have shown that these problems can be solved by the development of new materials [20–22]. For example, an organic material biochar exhibited outstanding performance in elimination of organic dye wastewater [23,24]. Chahinez et al. [25] prepared palm petiole biochar (DPP-biochar) and explored its adsorption mechanism for crystal violet (CV) dye, and the results showed that the amount of CV dye adsorbed on DPP-biochar increased from 18.8 to 27.4 mg/g within the increase of pH value from 2 to 12. Zhang et al. [26] used corncob as raw material to prepare biochar. It was found that the structure of biochar was similar to graphene, and the maximum adsorption capacity of molybdenum was 86.38 mg/g. In addition, biochar was also applied into agriculture, climate change mitigation and wastewater treatment due to its widespread sources, low production cost, diverse surface functional groups and easy surface modification [27–29]. However, the adsorption capacity of unmodified biochar was difficult to satisfy requirements of treatment, and many researchers began to explore how to improve its adsorption performance [30]. Some related researches have been reported. For example, the magnetic chitosan corn straw biochar was prepared by chemical co-precipitation method, and it could remove amaranth dye in solution. The maximum adsorption capacity could reach 404.18 mg/g [31]. Additionally, it was reported that the modified polythtyleneimine magnetic porous biochar from bamboo powder could also adsorb Congo red in solution. The adsorption capacity of Congo red by the modified biochar was high than the raw biochar [32]. Therefore, modified biochar are crucial to improve its performance [33].

In this study, it was focused on the preparation of biochar from peanut shells by method of microwave-assisted hydrothermal synthesis. Then it was loaded with Mg-Fe bimetallic oxides to form the novel composites (Mg-Fe@BC). The main objectives of this research were: (1) Preparation of Mg-Fe@BC composites; (2) Characterization of Mg-Fe@BC by scanning electron microscopy (SEM), transmission electron microscopy (TEM), energy-dispersive X-ray spectroscopy (EDS), Fourier-transform infrared spectroscopy (FTIR) and X-ray diffraction (XRD); (3) adsorption experiments of DR 167 dye by Mg-Fe@BC were carried out; (4) proposed mechanism of DR 167 dye by Mg-Fe@BC was discussed in details.

2. Material and methods

2.1. Chemicals and materials

Peanut shells were purchased from the farmers market (Shaoxing, China). All other chemicals, such as ferric chloride hexahydrate ($FeCl_3{\cdot}6H_2O$), magnesium chloride hexahydrate ($MgCl_2{\cdot}6H_2O$), NaOH, and DR 167 dye, were obtained from Macklin Biochemical Co., Ltd., (Shanghai, China). Additionally, they were all analytical reagents. The solutions required for the experiment were all prepared with ultrapure water. Structure of DR 167 dye is shown in Fig. 1.

2.2. Synthesis of biochar and Mg-Fe@BC

Preparation of biochar (BC): 1 g peanut shell powder (through 40 meshes) and 30 mL ultrapure water was mixed in 50 mL Teflon-digestion tank. Then, they were placed in microwave oven at a power of 80 W for 10 min. When it was cooled, the sample was washed by ultrapure water for three times. Next, they were dried to constant weight at 60°C. Then, BC was gained.

Preparation of Mg-Fe@BC: 18.92 g BC was dispersed in 100 mL Fe^{3+}/Mg^{2+} (n:n, 1:1), and then it was ultrasonically mixed for 10 min. Next, 100 mL 1 mol/L NaOH was added slowly. They were mixed for 2 h at 298 K and 200 rpm. Next, the obtained product was vacuum dried at 80°C for 12 h. Then, the Mg-Fe@BC composites were obtained.

2.3. Characterizations

The crystal structure of samples was analyzed by XRD. The scanning speed was 5 s per step and the 2θ range from 5 to 70, and λ was 1.5406 Å. Fourier-transform infrared spectroscopy (FTIR) was used to analyze the functional groups of the material. X-ray energy spectrum analysis (EDS) was carried out at 200 kV. Similarly, the morphology and structure distribution were characterized by scanning electron microscopy (SEM) (JEOL-6360LV, Japan) and transmission electron microscopy (TEM) (JEOL-JEM-1011, Japan) images.

2.4. Adsorption experiments

All the adsorption processes are carried out in 250 mL conical flasks with 100 mL of mixture and 150 rpm. The concentration of DR 167 dye is measured at 460 nm. The removal% (R) and adsorption capacity (q_e) of DR 167 dye at equilibrium are calculated with Eqs. (1) and (2), respectively. They are as follows:

$$R(\%) = \frac{(C_0 - C_e)}{C_0} \times 100\% \tag{1}$$

$$q_e(\text{mg/g}) = (C_0 - C_e) \times \frac{V}{m} \tag{2}$$

where C_0 (mg/L) and C_e (mg/L) are the initial concentration and equilibrium concentration of DR 167 dye; m (g) and V (L) are the mass and the volume of DR 167 dye, respectively; q_e (mg/g) is adsorption capacity at equilibrium.

3. Results and discussion

3.1. Characterization of BC and Mg-Fe@BC

As shown in Fig. 2a, it indicated that the surface of peanut shell biochar was smooth and porous structure. They were composed of macropores and micropores structures, and they were benefit to adsorb DR 167 dye [34]. The SEM image of Mg-Fe@BC showed that some generous rods of 75 nm were scattered on the surface of biochar.

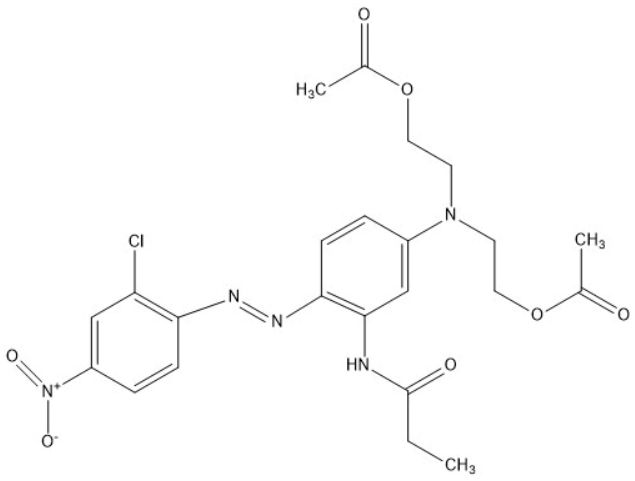

Fig. 1. Structure of DR 167 dye.

It could be concluded that Mg-Fe bimetallic oxide nanoparticles was appeared successfully on the surface of BC [35] (Fig. 2b). TEM images of BC and Mg-Fe@BC are depicted in Fig. 2c and d, respectively. It indicated that the composites of Mg-Fe bimetallic oxide nanoparticles were dispersed uniformly on the surface of BC.

For BC, EDS spectra was showed that the elements of C and O were appeared on the BC (Fig. 3). Their weight ratios were 56.45% and 43.55%, respectively. Additionally, for Mg-Fe@BC, the elemental distribution images of C, O, Mg and Fe are shown in Fig. 3. Their weight proportions were 45.22%, 32.17%, 3.15% and 19.46%, respectively. The above-mentioned elements were distributed evenly, and the composites contained multiple functional groups. Furthermore, the presence of iron and magnesium indicated that BC was successfully loaded by the composites of Mg-Fe@BC.

XRD pattern could be conducted to explore the crystal structure of BC and Mg-Fe@BC. It could be shown that the four characteristic peaks of BC at 15.6°, 22.1°, 26.4° and 34.6° could be observed (Fig. 4a). Additionally, seven characteristic peaks of Mg-Fe@BC at 15.1°, 22.3°, 27.5°, 31.7°, 34.7°, 45.4° and 56.6° could be observed, respectively. According to the diffraction pattern of BC, three new peaks at 31.7°, 45.4° and 56.6° could be observed, which were attributed to (220), (400) and (511) of $MgFe_2O_4$ cubic phase. It was similar with the results of other research [36].

FTIR of BC and Mg-Fe@BC are depicted in Fig. 4b. As shown from Fig. 4b, the characteristic peaks at 3,454–3,475; 1,630; 1,400; 1,051; 531 and 478 cm^{-1} appeared. They were corresponded to the O–H stretching vibration, the stretching vibration of C=C or C–C, the stretching vibration of COO^- and the stretching vibration of C–O–C, respectively [37]. In particular, the presence of the Mg–O and Fe–O stretching vibration indicated that Mg-Fe@BC was successfully synthesized [38].

In a word, according to the results of SEM, TEM, FTIR, XRD and EDS, it can be concluded that BC have been

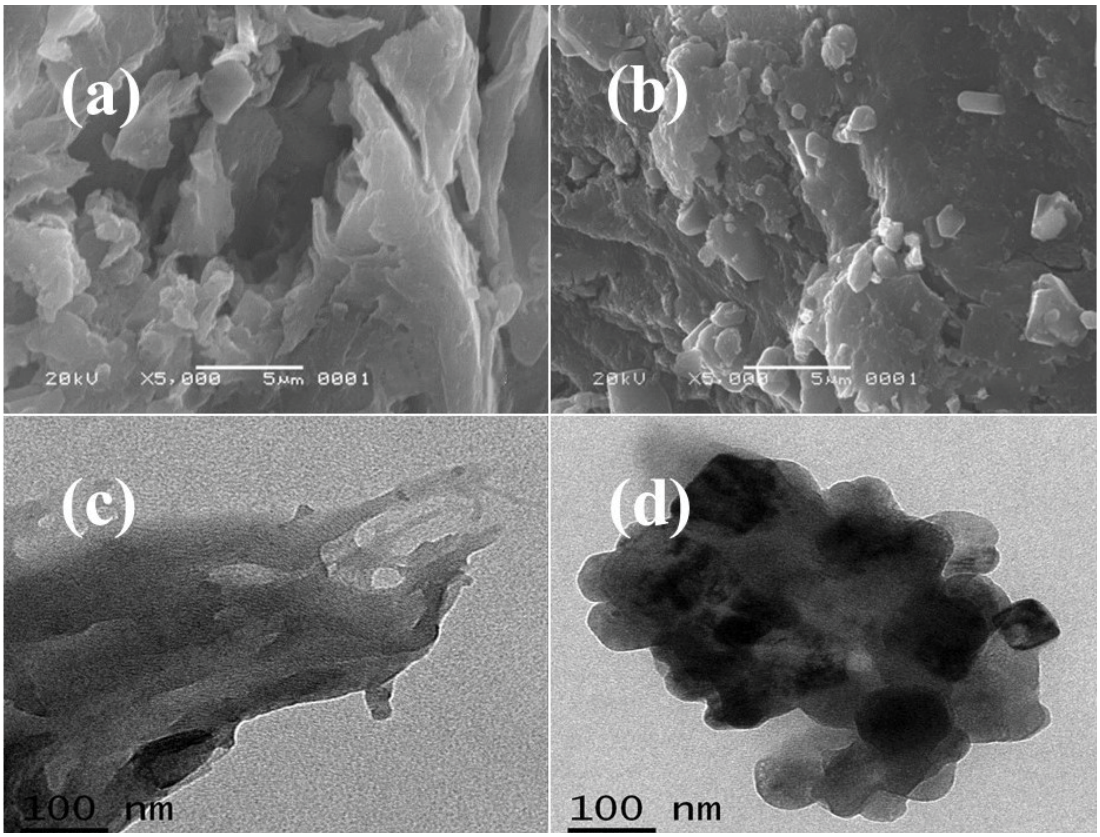

Fig. 2. SEM images of BC (a) and Mg-Fe@BC (b); TEM images of BC (c) and Mg-Fe@BC (d).

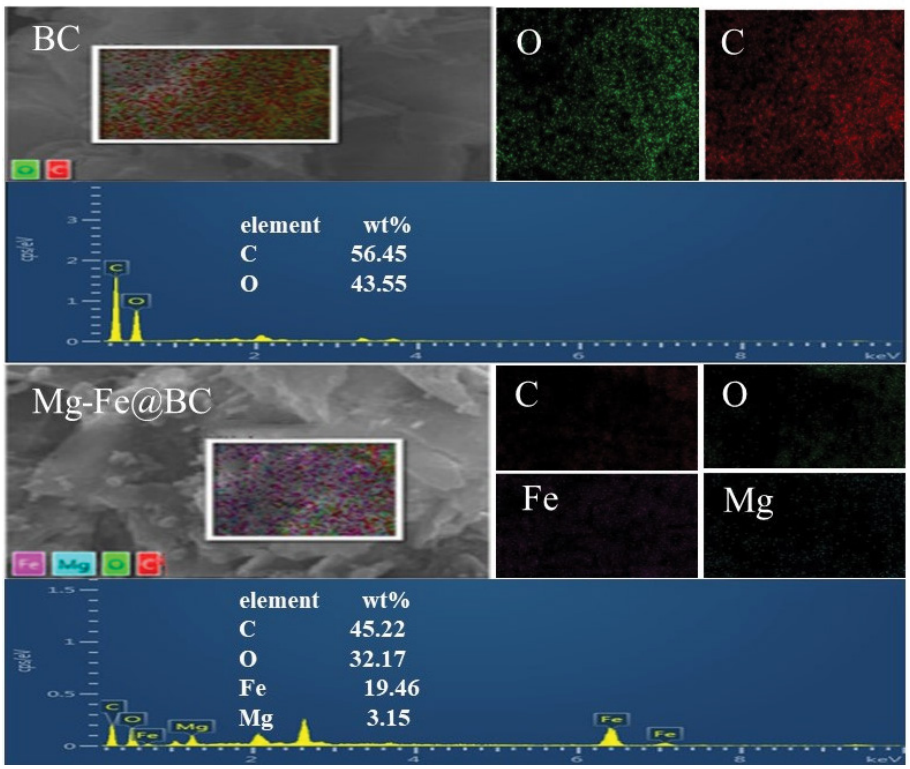

Fig. 3. EDS spectra of BC and Mg-Fe@BC.

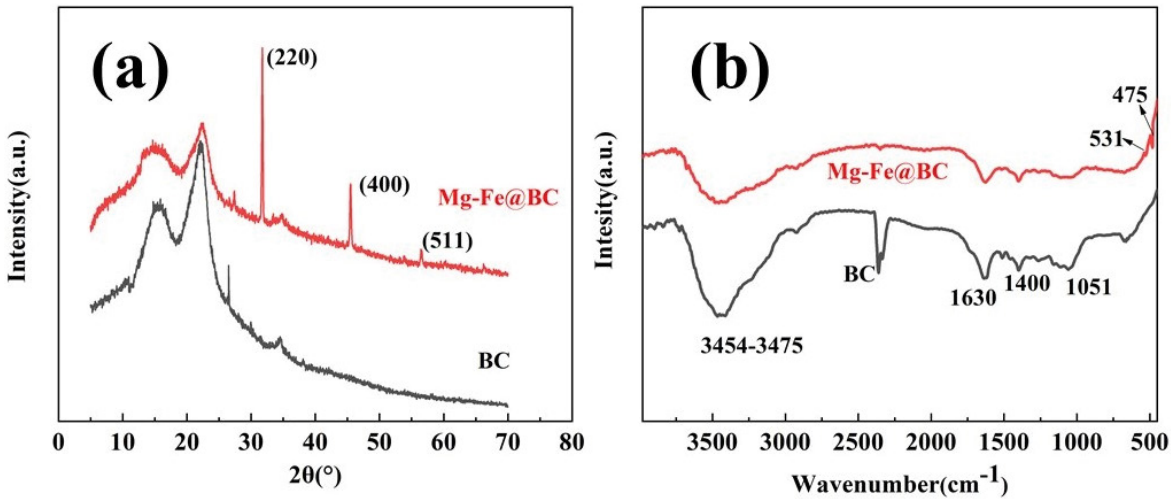

Fig. 4. (a) XRD pattern of BC and Mg-Fe@BC and (b) FTIR of BC and Mg-Fe@BC.

loaded by Mg/Fe compounds. The composite of Mg-Fe@BC was prepared perfectly.

3.2. Adsorption experiments

3.2.1. Effect of contact time

The effect of contact time on the adsorption of DR 167 dye was very important for the rapid removal of organic wastes from wastewater [39]. Therefore, the effect of contact time on DR 167 dye removal by BC and Mg-Fe@BC was tested [40]. As shown in Fig. 5a, the removal% of BC and Mg-Fe@BC increased with time at first of 60 min, and then remained stable. The rapid elimination of organic pollutants indicated that this stage was controlled by the charge on the surface of Mg-Fe@BC and the electrostatic attraction between DR 167 dye and BC or Mg-Fe@BC. However, the long-term elimination of organic pollutants indicated that this stage was mainly affected by the distribution of different sizes throughout the adsorption material.

3.2.2. Effect of initial pH

The pH in solution can reflect the binding ability of dye molecules to the surface of solid adsorbent. Additionally, it can also change the surface characteristics of solid adsorbent and the ionization or dissociation of dye molecules. Therefore, the pH in solution was an important parameter. Experiments were designed to determine the effect of pH on adsorption. The adsorption removal of DR 167 dye concentration of 60 mg/L by 0.1 g BC or Mg-Fe@BC was tested in pH 2, 4, 6, 8 and 10, respectively. According to Fig. 5b, with the increase of pH value, the adsorption rate decreased gradually. When the pH value was 2, the removal efficiency of BC and Mg-Fe@BC could reach 40.3% and 64.40%, respectively. The protonation of functional groups on the surface of biochar and its modified materials could remove DR 167 dye through electrostatic attraction. Therefore, it could further promote the reduction and fracture process of dual nitrogen bond in dye molecules [41].

$$Fe^{2+} - e^{-} \rightarrow Fe^{3+} \quad (3)$$

$$-N{=}N- + 2H^{+} + 2e^{-} \rightarrow 2HN- \quad (4)$$

3.2.3. Effect of temperature and dye concentration

The temperature had a great influence on the adsorption of DR 167 dye. The removal rate of DR 167 dye by BC and Mg-Fe@BC was increased in the temperature range of 298 to 318 K. It was found that the adsorption capacities of DR 167 dye by BC and Mg-Fe@BC were 30.245 and 50.429 mg/g at 298 K, respectively. However, adsorption capacity of DR 167 dye by BC and Mg-Fe@BC increased significantly to 50.124 and 68.134 mg/g at 318 K, respectively. It indicated that the adsorption of DR 167 dye by BC and Mg-Fe@BC was endothermic process (Fig. 6a). It might be due to the increase of the solubility of DR 167 dye and interaction between DR 167 dye and adsorbent. As shown in Fig. 6b,

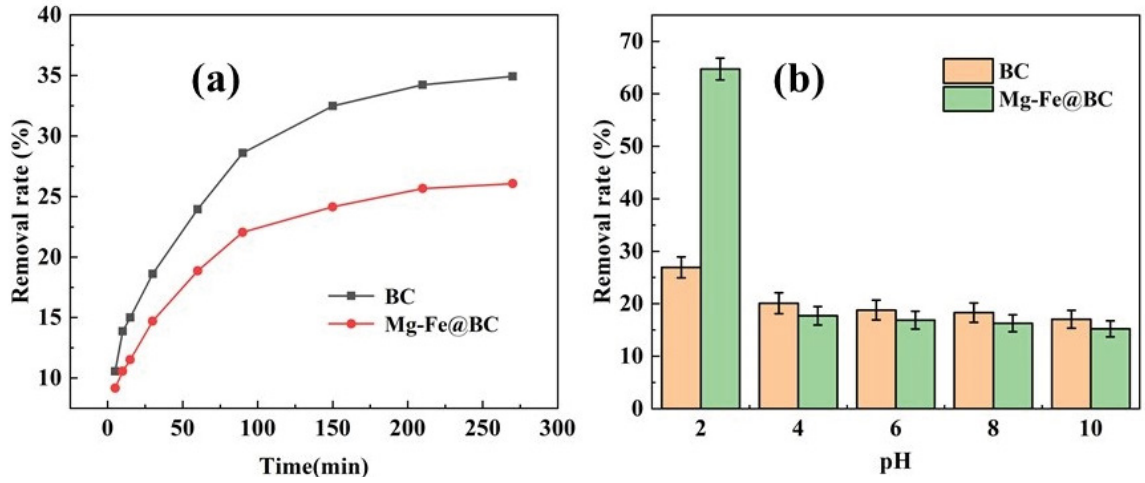

Fig. 5. Effect of contact time (a) and initial pH in solution (b).

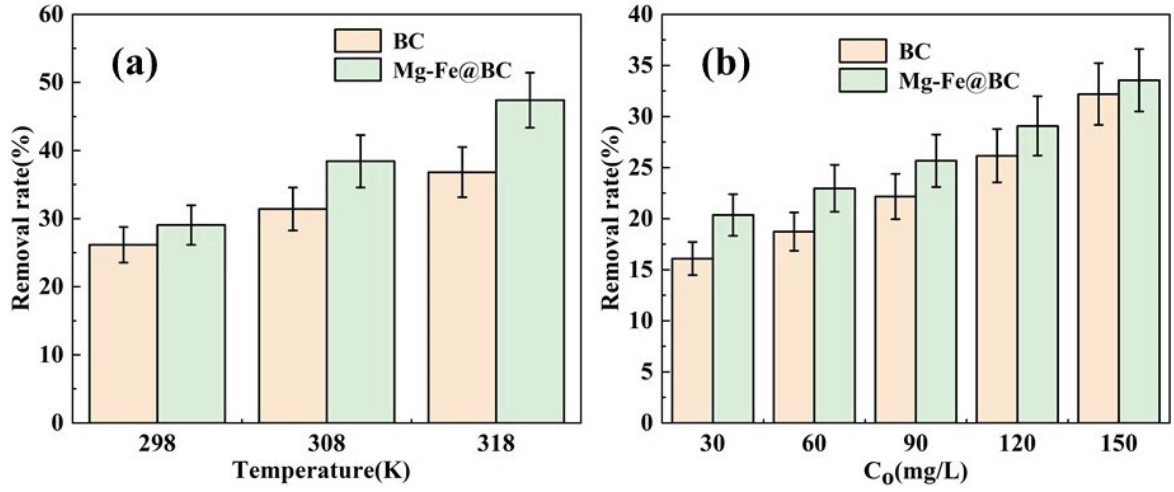

Fig. 6. Effect of temperature (a) and concentration of DR 167 dye (b).

the removal capacity of different dye concentration by BC and Mg-Fe@BC decreased with the decrease of concentration. It might be due to reduce of dye concentration, which inhibited the contact between adsorbent and DR 167 dye.

3.2.4. Isotherm, kinetic and thermodynamic

The isotherm reaction was the adsorption degree of solute between the interface of two phases, when the equilibrium state was reached at a specific temperature [42,43]. In this research, the classic Langmuir and Freundlich isotherm models [44] were used. The adsorption isotherms of DR 167 dye were obtained at 298, 308 and 318 K.

Langmuir model [Eq. (5)] was assumed that the adsorbate was monolayer adsorption, and there was no interaction between the adsorbate and uniform adsorption energy on the adsorbent surface [45].

$$q_e = \frac{Q_{\max} K_L C_e}{1 + K_L C_e} \tag{5}$$

where C_e is the concentration of the solution at equilibrium, mg/L. q_e and $Q_{\max}$ are the amount of dye adsorbed at equilibrium and the maximum amount of dye adsorbed on the adsorbent, mg/g. K_L is expressed as Langmuir constant, which is related to the free energy of adsorption.

The Freundlich model [Eq. (6)] is a semi empirical equation, which indicates the heterogeneous surface of multilayer adsorption and adsorbent [46].

$$q_e = K_F C_e^{1/n} \tag{6}$$

where, q_e is the adsorption capacity at equilibrium, mg/g. C_e is the dye concentration at equilibrium, mg/L. K_F is the Freundlich adsorption equilibrium constant, mg/g. n is the heterogeneity factor related to the sorption intensity. Sorption isotherms of DR 167 dye removal by BC and Mg-Fe@BC are shown in Fig. 7.

From Fig. 7, when temperature increased, the adsorption capacity also increased. It indicated that temperature could promote the adsorption of DR 167 dye. According to the results of Fig. 7 and Eqs. (5) and (6), the related parameters of Langmuir and Freundlich models could be calculated (Table 1).

As shown in Table 1, the R^2 values of BC and Mg-Fe@BC for Langmuir adsorption model were 0.9987 and 0.9994, respectively, which were higher than those for Freundlich adsorption model. It was suggested that the adsorption

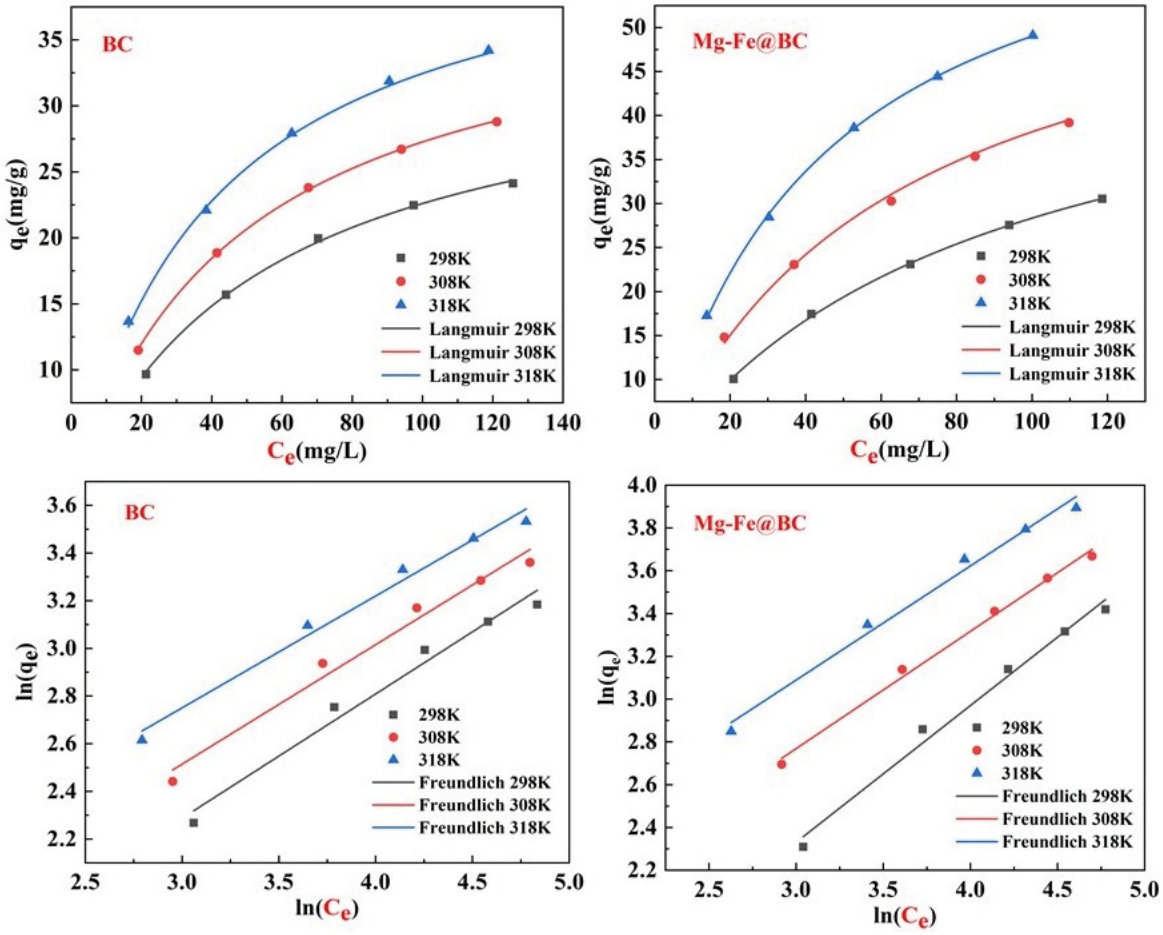

Fig. 7. Sorption isotherms of DR 167 dye removal by BC and Mg-Fe@BC.

Table 1
The parameters of DR 167 dye removal by BC and Mg-Fe@BC

Adsorbents	T(K)	Langmuir model			Freundlich model		
		Q_{max} (mg/g)	K_L (L/mg)	R^2	K_F (mg^{1-n} L^n g^{-1})	n	R^2
BC	298	34.743	0.0186	0.9987	1.5132	1.5652	0.977
	308	40.045	0.0213	0.9997	2.0602	1.8247	0.979
	318	45.264	0.0253	0.9984	2.7453	1.8747	0.985
Mg-Fe@BC	298	52.855	0.0115	0.9994	3.0783	1.9179	0.987
	308	62.010	0.0159	0.9960	3.8272	1.9948	0.994
	318	70.457	0.0228	0.9996	4.4305	2.1306	0.988

of dye in aqueous solution was monolayer. The maximum adsorption capacity of BC at 298 K was 34.734 mg/g, and Mg-Fe@BC was 52.855 mg/g at 298 K. It was consistent with the actual experimental results. In addition, Mg-Fe@BC composites showed excellent adsorption properties under similar conditions. It indicated that the composites could be considered as efficient, environmentally friendly and low-cost dye removal materials.

In order to understand the mechanism of adsorption of DR 167 dye by BC and Mg-Fe@BC, the experimental kinetic data were fitted to two models of pseudo-first-order and pseudo-second-order. The two models can be represented by the following equations:

$$\ln\left(q_e - q_t\right) = \ln q_e - k_1 t \tag{7}$$

$$\frac{t}{q_t} = \frac{1}{k_2 \times q_e^2} + \frac{t}{q_e} \tag{8}$$

where q_e and q_t are the adsorption capacity at equilibrium time and different time, mg/g, respectively. k_1 is the constant (min^{-1}), and k_2 also is constant (g/(mg min)).

The removal efficiency of DR 167 dye by Mg-Fe@BC was better than that of BC (Fig. 8). The adsorption kinetic parameters of DR 167 dye by BC and Mg-Fe@BC are shown in Table 2. The results showed that the pseudo-second-order model of Mg-Fe@BC had a higher R^2 value than the pseudo-first-order model. It indicated that the adsorption kinetic parameters of DR 167 dye were more consistent with the pseudo-second-order model. It could be concluded that the modified biochar was mainly controlled by chemical adsorption [47].

In this work, the thermodynamic behavior was investigated at 25°C, 35°C and 45°C, respectively. The thermodynamic parameters of adsorption of DR 167 dye by BC and Mg-Fe@BC are calculated by Eqs. (9)–(11).

$$k_c = \frac{q_e}{C_e} \tag{9}$$

$$\Delta G° = -RT\ln\left(k_c\right) \tag{10}$$

$$\ln\left(k_c\right) = \frac{-\Delta H°}{R}\frac{1}{T} + \frac{\Delta S°}{R} \tag{11}$$

where k_c is the balance parameter, L/mg, and q_e is adsorption amount of DR 167 dye at equilibrium, mg/g. C_e is concentration of DR 167 dye at equilibrium, mg/L. $\Delta G°$ is Gibbs free energy of adsorption, kJ/mol. $\Delta H°$ is enthalpy, kJ/mol and $\Delta S°$ are entropy, J/(mol/k). R was the gas parameter, J/(k mol), and T is the absolute temperature of adsorption, K.

Fig. 8 shows that temperature had a great influence on the adsorption mechanism of dye removal. When temperature was increased, the adsorption capacity of DR 167 dye increased. The thermodynamic parameters of DR 167 dye were given in Table 3. For BC, the value of $\Delta H°$ and $\Delta S°$ was 12.099 kJ/mol and 0.064 J/mol/K, respectively. For Mg-Fe@BC, the value of $\Delta H°$ and $\Delta S°$ was 22.219 kJ/mol and 0.104 J/mol/K, respectively. The positive value of $\Delta H°$ and $\Delta S°$ indicated that the adsorption process was endothermic. It depicted that the increase of reaction temperature was conductive to the reaction. Negative results of $\Delta G°$ indicated that the adsorption was spontaneous. Furthermore, the $\Delta G°$ value decreased with the increase of temperature, which indicated that the higher the temperature was instrumental in adsorption process. Therefore, it was spontaneous and endothermic process.

3.3. Possible of adsorption mechanism

According the results of FTIR for Mg-Fe@BC, the strong characteristic peaks at 3,454–3,475 cm^{-1} and 1,400 cm^{-1} are

Table 2
The parameters of kinetic models of DR 167 dye adsorption on BC and Mg-Fe@BC

Adsorbents	Pseudo-first-order model			Pseudo-second-order model		
	k_1 (min^{-1})	q_e (mg/g)	R^2	k_2 (g/mg min)	q_e (mg/g)	R^2
BC	0.0275	15.2946	0.9624	0.0011	21.524	0.9996
Mg-Fe@BC	0.0328	19.2968	0.995	0.00032	38.462	0.9993

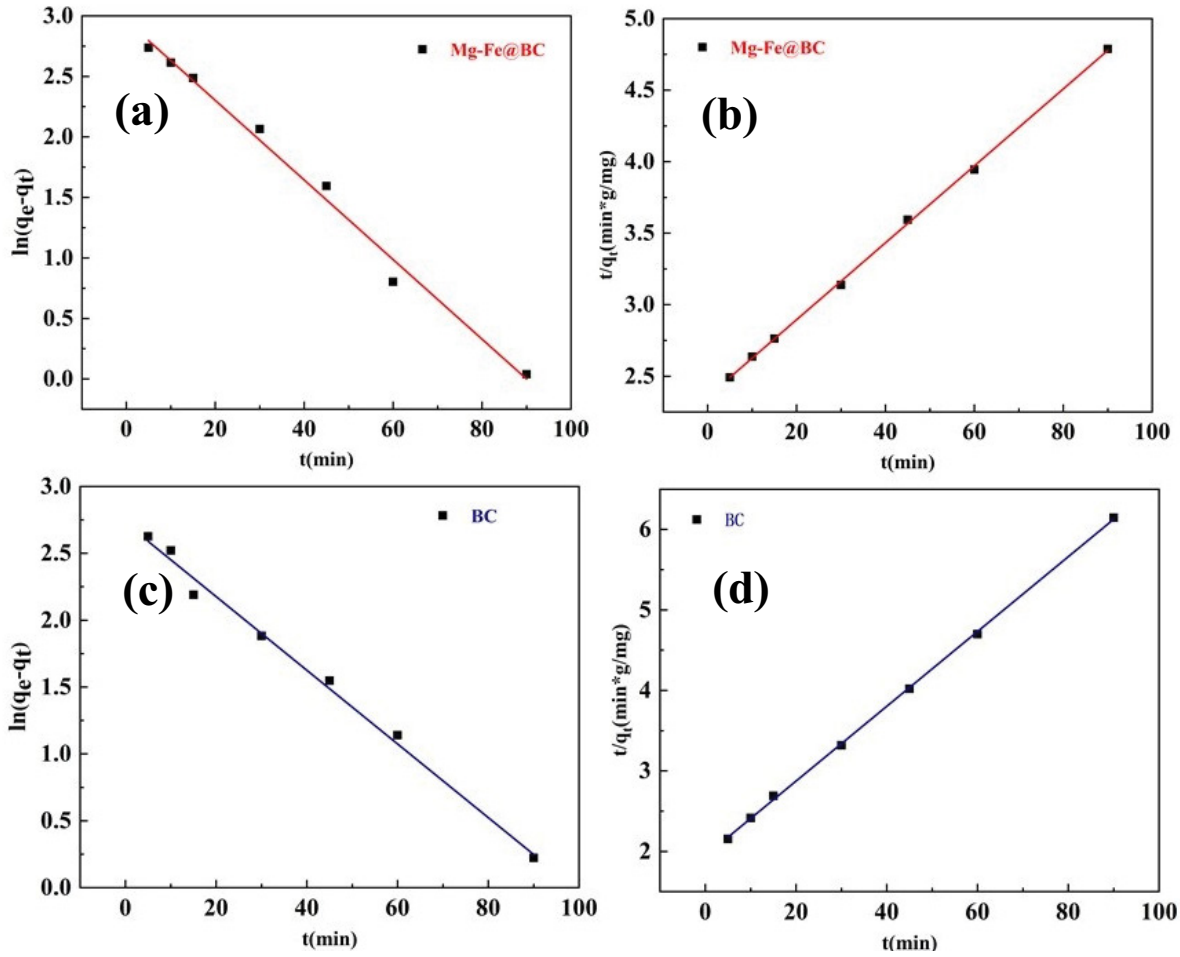

Fig. 8. First-second-order model of DR 167 dye adsorption by Mg-Fe@BC (a) and BC (c); pseudo-second-order model of DR 167 dye adsorption by Mg-Fe@BC (b) and BC (d).

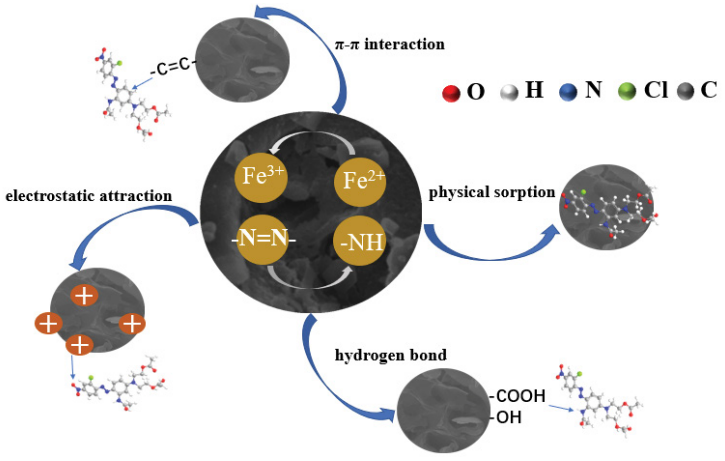

Fig. 9. The possible mechanism of removing DR 167 dye by Mg-Fe@BC.

related to the stretching vibration of –OH and –COOH, respectively. These functional groups can adsorb the adsorption of dyes. The groups of hydroxyl and carboxyl could adsorb dye through electrostatic attraction [48]. On the other hand, it could form hydrogen bond with nitrogen in the dye to promote the adsorption process. The results of XRD and SEM showed that a lot of Fe^{2+} ions appeared on the surface of Mg-Fe@BC. Iron could promote the increase

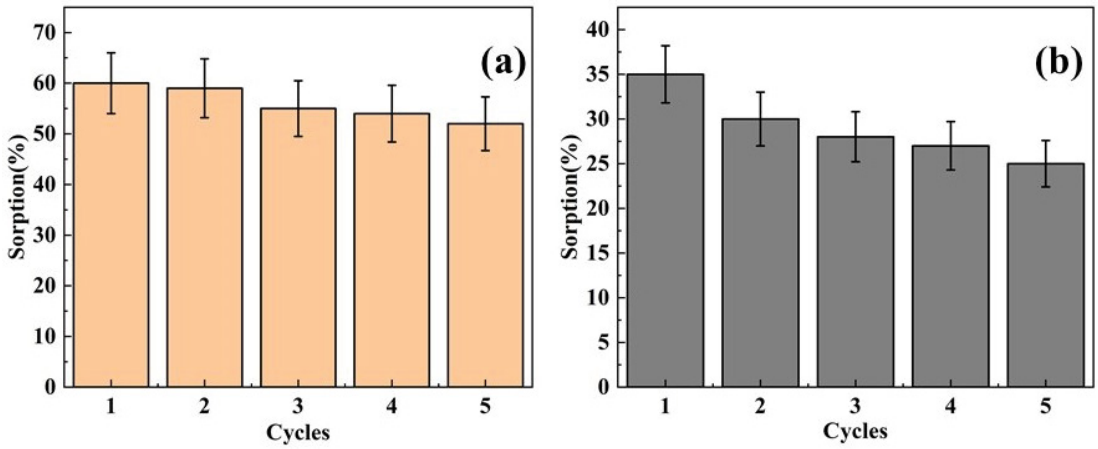

Fig. 10. Recycling of Mg-Fe@BC (a) and BC (b) for DR 167 dye removal.

Table 3
Thermodynamics parameters of DR 167 dye removal by BC and Mg-Fe@BC

Adsorbents	T(K)	$\Delta G°$	$\Delta H°$	$\Delta S°$
		kJ/mol	kJ/mol	J/mol/K
BC	298	–5.541	12.099	0.064
	308	–6.087		
	318	–6.740		
Mg-Fe@BC	298	–4.362	22.219	0.104
	308	–5.338		
	318	–6.465		

of oxygen-containing functional groups and improve the stability of the reaction π–π interaction between dye DR 167 and Mg-Fe@BC [49–51].

Therefore, the possible mechanism of DR 167 dye removal by Mg-Fe@BC is shown in Fig. 9. From Fig. 9 it can be concluded that the mechanism of DR 167 dye removal by Mg-Fe@BC involved electrostatic attraction, hydrogen bonding, surface complexation and π–π interactions.

3.4. Reusability experiment

The ability of recycle was very important for the efficient bio-adsorbent in order to improve the economic value of the reaction process. The adsorption–desorption experiment was carried out. In this study, the adsorbed material was desorbed with ethanol solution, and the reusability experiment was tested for five consecutive cycles (Fig. 10). The results showed that the adsorption capacity of BC and Mg-Fe@BC had little change in multiple adsorption–desorption experiments, which further revealed the high reusability of biochar and its modified materials.

4. Conclusions

In this research, the composites of Mg-Fe@BC were synthesized by the method of microwave-assisted. The removal rate of DR 167 dye removal by Mg-Fe@BC could reach 92.7%. The experimental equilibrium data revealed that the removal efficiency of DR 167 dye by Mg-Fe@BC was better than that of the original biochar, and the adsorption process was best-fitted pseudo-second-order and Langmuir model, respectively. It indicated that the adsorption was mainly chemical and monolayer. Additionally, the adsorption mechanisms of DR 167 dye removal by Mg-Fe@BC involved electrostatic attraction, hydrogen bonding, surface complexation and π–π interactions.

Acknowledgements

This research was supported by Zhejiang Provincial Natural Science Foundation of China (LGF20C030001 and LZY21C030001).

References

[1] C.L. Jiang, X.H. Wang, D.M. Qin, W.X. Da, B.X. Hou, C. Hao, J.B. Wu, Construction of magnetic lignin-based adsorbent and its adsorption properties for dyes, J. Hazard. Mater., 369 (2019) 50–61.
[2] M.Q. Qiu, Z.X. Liu, S.Q. Wang, B.W. Hu, The photocatalytic reduction of U(VI) into U(IV) by ZIF-8/g-C_3N_4 composites at visible light, Environ. Res., 196 (2021) 110349, doi: 10.1016/j.envres.2020.110349.
[3] Y.B. Qiu, Y.Y. Lv, C. Tang, J.B. Liao, H.M. Ruan, S. Arcadio, J.N. Shen, Sustainable recovery of high-saline papermaking wastewater: optimized separation for salts and organics via membrane-hybrid process, Desalination, 507 (2021) 114938, doi: 10.1016/j.desal.2021.114938.
[4] N. Cao, C. Yue, Z.Y. Lin, Z.Y. Li, H.B. Zhang, J.H. Pang, Z.H. Jiang, Durable and chemical resistant ultra-permeable nanofiltration membrane for the separation of textile wastewater, J. Hazard. Mater., 414 (2021) 125489, doi: 10.1016/j.jhazmat.2021.125489.
[5] Y.K. Choi, T.R. Choi, R. Gurav, S.K. Bhatia, Y.L. Park, H.J. Kim, E. Kan, Y.H. Yang, Adsorption behavior of tetracycline onto *Spirulina* sp. (microalgae)-derived biochars produced at different temperatures, Sci. Total Environ., 710 (2020) 136282, doi: 10.1016/j.scitotenv.2019.136282.
[6] M.Q. Qiu, M. Wang, Q.Z. Zhao, B.W. Hu, Y.L. Zhu, XANES and EXAFS investigation of uranium incorporation on nZVI in the presence of phosphate, Chemosphere, 201 (2018) 764–771.

[7] W.X. Zhou, X.G. Chen, M. Ismail, L. Wei, B.L. Hu, Simulating the synergy of electron donors and different redox mediators on the anaerobic decolorization of azo dyes: Can AQDS-chitosan globules replace the traditional redox mediators?, Chemosphere, 275 (2021) 130025, doi: 10.1016/j.chemosphere.2021.130025.
[8] H. Xu, B. Yang, Y.B. Liu, F. Li, C.S. Shen, C.Y. Ma, Q. Tian, X.S. Song, W. Sand, Recent advances in anaerobic biological processes for textile printing and dyeing wastewater treatment: a mini-review, World J. Microbiol. Biotechnol., 34 (2018) 165, doi: 10.1007/s11274-018-2548-y.
[9] S. Mishra, L. Cheng, A. Maiti, The utilization of agro-biomass/byproducts for effective bio-removal of dyes from dyeing wastewater: a comprehensive review, J. Environ. Chem. Eng., 9 (2021) 104901, doi: 10.1016/j.jece.2020.104901.
[10] C.R. Holkar, A.B. Pandit, D.V. Pinjari, Kinetics of biological decolorisation of anthraquinone based Reactive Blue 19 using an isolated strain of *Enterobacter* sp.F NCIM 5545, Bioresour. Technol., 173 (2014) 342–351.
[11] K.M. Zhu, X.S. Wang, D. Chen, W. Ren, H. Lin, H. Zhang, Wood-based biochar as an excellent activator of peroxydisulfate for Acid Orange 7 decolorization, Chemosphere, 231 (2019) 32–40.
[12] M. Altikatoglu, M. Celebi, Enhanced stability and decolorization of Coomassie Brilliant Blue R-250 by dextran aldehyde-modified horseradish peroxidase, Artif. Cells, Blood Substitues, Immobilization Biotechnol., 39 (2011) 185–190.
[13] G. Bayramoglu, G. Kunduzcu, M.Y. Arica, Preparation and characterization of strong cation exchange terpolymer resin as effective adsorbent for removal of disperse dyes, Polym. Eng. Sci., 60 (2019) 192–201.
[14] M. Goswami, P. Chaturvedi, R.K. Sonwani, A.D. Gupta, R.R. Singhania, B.S. Giri, B.N. Rai, H. Singh, S. Yadav, R.S. Singh, Application of Arjuna (*Terminalia arjuna*) seed biochar in hybrid treatment system for the bioremediation of Congo red dye, Bioresour. Technol., 307 (2020) 123203, doi: 10.1016/j.biortech.2020.123203.
[15] T. Kim, B.J. Seo, G.H. Park, Y.W. Lee, Predicting diffusion behavior of disperse dyes in polyester fibers by a method based on extraction, J. Supercrit. Fluids, 157 (2020) 104685, doi: 10.1016/j.supflu.2019.104685.
[16] F.Y. Li, F.L. Duan, W.C. Ji, X.Y. Gui, Biochar-activated persulfate for organic contaminants removal: Efficiency, mechanisms and influencing factors, Ecotoxicol. Environ. Saf., 198 (2020) 110653, doi: 10.1016/j.ecoenv.2020.110653.
[17] J.F. Chen, H.W. Hu, J.H. Yang, H.H. Xue, Y.P. Tian, K.Y. Fan, Z.X. Zeng, J.Q. Yang, R.J. Wang, Y.Y Liu, Removal behaviors and mechanisms for series of azo dye wastewater by novel nano constructed macro-architectures material, Bioresour. Technol., 322 (2021) 124556, doi: 10.1016/j.biortech.2020.124556.
[18] M. Israr, J. Iqbal, A. Arshad, P.G. Romero, B. Benages, Multifunctional $MgFe_2O_4$/GNPs nanocomposite: graphene-promoted visible light driven photocatalytic activity and electrochemical performance of $MgFe_2O_4$ nanoparticles, Solid State Sci., 110 (2020) 106363, doi: 10.1016/j.solidstatesciences.2020.106363.
[19] X.M. Tang, T. Wang, S.X. Zhang, L. Fang, H.L. Zheng, Enhanced performance of a novel flocculant containing rich fluorine groups in refractory dyeing wastewater treatment: removal mechanisms, Sep. Purif. Technol., 263 (2021) 118411, doi: 10.1016/j.seppur.2021.118411.
[20] S. Meng, S.L. Yu, F.Y. Tang, X.N. Hu, J. Lu, X. Fei, M.F. Zhu, Fiber engineering of silica-based aerogels with surface specificity and regenerability for continuous removal of dye pollutants from wastewaters, Microporous Mesoporous Mater., 314 (2021) 110874, doi: 10.1016/j.micromeso.2021.110874.
[21] K.T. Kubra, M.S. Salman, M.N. Hasan, Enhanced toxic dye removal from wastewater using biodegradable polymeric natural adsorbent, J. Mol. Liq., 328 (2021) 115468, doi: 10.1016/j.molliq.2021.115468.
[22] S. Senguttuvan, P. Senthilkumar, V. Janaki, K. Kanan, Significance of conducting polyaniline based composites for the removal of dyes and heavy metals from aqueous solution and wastewaters – a review, Chemosphere, 267 (2021) 129201, doi: 10.1016/j.chemosphere.2020.129201.
[23] G. Chu, J. Zhao, F.Y. Chen, X.D. Dong, D.D. Zhou, N. Liang, M. Wu, B. Pan, E.W.S. Christian, Physi-chemical and sorption properties of biochars prepared from peanut shell using thermal pyrolysis and microwave irradiation, Environ. Pollut., 227 (2017) 372–379.
[24] M. Vithanage, A. Ashiq, S. Ramanayaka, A. Bhatnagar, Implications of layered double hydroxides assembled biochar composite in adsorptive removal of contaminants: current status and future perspectives, Sci. Total Environ., 737 (2020) 139718, doi: 10.1016/j.scitotenv.2020.139718.
[25] H.O. Chahinez, O. Abdelkader, Y. Leila, H.N. Tran, One-stage preparation of palm petiole-derived biochar: characterization and application for adsorption of crystal violet dye in water, Environ. Technol. Innovation, 19 (2020) 100872, doi: 10.1016/j.eti.2020.100872.
[26] Z. Zhang, G.H. Wang, W.B. Li, L.D. Zhang, T. Chen, L. Ding, Degradation of methyl orange through hydroxyl radical generated by optically excited biochar: performance and mechanism, Colloids Surf., A, 601 (2020) 125034, doi: 10.1016/j.colsurfa.2020.125034.
[27] S. Rodrigues, E. Horan, The Role of Biochar in Sustainable Agriculture, and Climate Change Mitigation for Sustainable Cities, In: Sustainable Development Research in the Asia-Pacific Region, Springer, 2018, pp. 437–447.
[28] M.J. Hao, M.Q. Qiu, H. Yang, B.W. Hu, X.X. Wang, Recent advances on preparation and environmental applications of MOF-derived carbons in catalysis, Sci. Total Environ., 760 (2021) 143333, doi: 10.1016/j.scitotenv.2020.143333.
[29] B.W. Hu, H.F. Wang, R.R. Liu, M.Q. Qiu, Highly efficient U(VI) capture by amidoxime/carbon nitride composites: evidence of EXAFS and modeling, Chemosphere, 274 (2021) 129743, doi: 10.1016/j.chemosphere.2021.129743.
[30] R. Gurav, S.K. Bhatia, T.R. Choi, Y.K. Choi, H.J. Kim, H.S. Song, S.M. Lee, S.L. Park, H.S. Lee, J. Koh, J.M. Jeon, J.J. Yoon, Y.H. Yang, Application of macroalgal biomass derived biochar and bioelectrochemical system with *Shewanella* for the adsorptive removal and biodegradation of toxic azo dye, Chemosphere, 264 (2021) 128539, doi: 10.1016/j.chemosphere.2020.128539.
[31] F. Wang, L. Li, J.R. Iqbal, Z.R. Yang, Y.P. Du, Preparation of magnetic chitosan corn straw biochar and its application in adsorption of amaranth dye in aqueous solution, Int. J. Biol. Macromol., 199 (2022) 234–242.
[32] Z.D. Wu, X.M. Wang, J. Yao, S.Y. Zhan, H. Li, J. Zhang, Z.M. Qiu, Synthesis of polyethyleneimine modified $CoFe_2O_4$-loaded porous biochar for selective adsorption properties towards dyes and exploration of interaction mechanisms, Sep. Purif. Technol., 277 (2021) 119474, doi: 10.1016/j.seppur.2021.119474.
[33] K.S.D. Premarathna, A.U. Rajapaksha, B. Sarkar, E.E. Kwon, A. Bhatnagar, Y.S. Ok, M. Vithanage, Biochar-based engineered composites for sorptive decontamination of water: a review, Chem. Eng. J., 372 (2019) 536–550.
[34] J.E. Kim, S.K. Bhatia, H.J. Song, E.J. Yoo, Y.K. Choi, Adsorptive removal of tetracycline from aqueous solution by maple leaf-derived biochar, Bioresour. Technol., 306 (2020) 123092, doi: 10.1016/j.biortech.2020.123092.
[35] M. Adel, M.A. Ahmed, A.A. Mohamed, Synthesis and characterization of magnetically separable and recyclable crumbled $MgFe_2O_4$/reduced graphene oxide nanoparticles for removal of methylene blue dye from aqueous solutions, J. Phys. Chem. Solids, 149 (2021) 109760, doi: 10.1016/j.jpcs.2020.109760.
[36] X.H. Wang, X.C. Kan, X.S. Liu, S. Feng, C. Liu, Characterization of microstructure and magnetic properties for Co_2^+ ions doped $MgFe_2O_4$ spinel ferrites, Mater. Today Commun., 25 (2020) 101414, doi: 10.1016/j.mtcomm.2020.101414.
[37] L. Fang, J.S. Li, S. Donatello, C.R. Cheeseman, D.C.W. Tsang, Use of Mg/Ca modified biochars to take up phosphorus from acid-extract of incinerated sewage sludge ash (ISSA) for fertilizer application, J. Cleaner Prod., 244 (2020) 118853, doi: 10.1016/j.jclepro.2019.118853.

[38] M. Thangaraj, G. Vinitha, T.S. Girisun, P. Anandan, G. Ravi, Third order nonlinear optical properties and optical limiting behavior of alkali metal complexes of p-nitrophenol, Opt. Laser Technol., 73 (2016) 130–134.
[39] S.Y. Yang, Q. Li, L. Chen, Z. Chen, X. Wang, Ultrahigh sorption and reduction of Cr(VI) by two novel core-shell composites combined with Fe_3O_4 and MoS_2, J. Hazard. Mater., 379 (2019) 120797, doi: 10.1016/j.jhazmat.2019.120797.
[40] G. Bayramoglu, M.Y. Arica, Star type polymer grafted and polyamidoxime modified silica coated-magnetic particles for adsorption of U(VI) ions from solution, Chem. Eng. Res. Des., 147 (2019) 146–159.
[41] M. Barreto-Rodrigues, J. Silveira, J.A. Zazo, J.J. Rodriguez, Synthesis, characterization and application of nanoscale zero-valent iron in the degradation of the azo dye Disperse Red 1, J. Environ. Chem. Eng., 5 (2017) 628–634.
[42] B. Priyadarshini, T. Patra, T.R. Sahoo, An efficient and comparative adsorption of Congo red and Trypan blue dyes on MgO nanoparticles: kinetics, thermodynamics and isotherm studies, J. Magnesium Alloys, 16 (2020) 1–11.
[43] H. Haroon, J.A. Shah, M.S. Khan, T. Naqvi, M. Bilal, Activated carbon from a specific plant precursor biomass for hazardous Cr(VI) adsorption and recovery studies in batch and column reactors: isotherm and kinetic modeling, J. Water Process Eng., 38 (2020) 101557, doi: 10.1016/j.jwpe.2020.101577.
[44] J. Duan, H.D. Ji, T.Y. Xu, F. Pan, Simultaneous adsorption of uranium(VI) and 2-chlorophenol by activated carbon fiber supported/modified titanate nanotubes (TNTs/ACF): effectiveness and synergistic effects, Chem. Eng. J., 406 (2020) 126752, doi: 10.1016/j.cej.2020.126752.
[45] L. Wang, L.Y. Yuan, K. Chen, Y. Zhang, Q. Deng, S. Du, Q. Huang, L. Zheng, J. Zhang, Z. Chai, Loading actinides in multilayered structures for nuclear waste treatment: the first case study of uranium capture with vanadium carbide MXene, ACS Appl. Mater. Interfaces, 8 (2016) 16396–16403.
[46] P. Amesh, A.S. Suneesh, K.A. Venkatesan, M. Chandra, N.A. Ravindranath, High capacity amidic succinic acid functionalized mesoporous silica for the adsorption of uranium, Colloids Surf., A, 602 (2020) 125053, doi: 10.1016/j.colsurfa.2020.125053.
[47] Q.Q. Yin, R.K. Wang, Z.H. Zhao, Application of Mg–Al-modified biochar for simultaneous removal of ammonium, nitrate, and phosphate from eutrophic water, J. Cleaner Prod., 176 (2018) 230–240.
[48] L. Lonapan, T. Rouissi, S.K. Brar, M. Verma, Y.S. Rao, An insight into the adsorption of diciofence on different biochars: mechanisms, surface chemistry, and thermodynamics, Bioresour. Technol., 249 (2018) 386–394.
[49] X. Ruan, Y.Y. Liu, G.P. Wang, R.L. Frost, G. Qian, D.C.W. Tsang, Transformation of functional groups and environmentally persistent free radicals in hydrothermal carbonisation of lignin, Bioresour. Technol., 270 (2018) 223–229.
[50] J.H. Kim, S.H. Hyun, Sorption of ionic and nonionic organic solutes onto giant *Miscanthus*-derived biochar from methanol-water mixtures, Sci. Total Environ., 615 (2018) 805–813.
[51] P. Sirajudheen, M.R. Nikitha, P. Karthikeyan, S. Meenashi, Perceptive removal of toxic azo dyes from water using magnetic Fe_3O_4 reinforced graphene oxide–carboxymethyl cellulose recyclable composite: adsorption investigation of parametric studies and their mechanisms, Surf. Interfaces, 21 (2020) 100648, doi: 10.1016/j.surfin.2020.100648.